

Cascade system using both trough system and dish system for power generation

Abstract

This paper represents an idea of cascade collection and cascade utilization of solar energy with higher efficiency. Parabolic trough collectors are used to collect lower temperature energy and dish collectors are used to collect higher temperature energy, Rankine cycle is used to work in lower temperature zone and Stirling cycle is used to work in higher temperature zone. An effective structure using the condensed fluid of Rankine cycle to cool the Stirling engines to use the heat released by Stirling engines was proposed. A cascade system model including different fluid circuits with component models was established. Simulations were conducted with design parameters. The model of some important components of the system, such as dish collector, trough collector and Stirling engine array, are presented with detail explanation in this paper. Corresponding separate systems were also established for comparison. Results show that the cascade system can achieve a higher efficiency under certain conditions. The directions to increase the efficiency difference between cascade system and corresponding separate systems were also considered. Higher irradiance and Stirling engine ratio is better for a cascade system. The flow type of fluids between heating and cooling Stirling engine array is also required to concern on designing a cascade system with Stirling engine array.

Keywords: cascade system, dish receiver, trough collector, Stirling engine array

1 Introduction

Energy is the crucial part for the infrastructure and maintenance of society. With the increase amount of energy consumption, our quality of life has been improved significantly. However, nowadays the world energy consumption is highly dependent on fossil fuels, which supplied 81.3% of the world's energy consumption in 2012 according to the data of World Bank Group. Using fossil fuels a lot is afflicting the environment, which is sacrificing our quality of life. Environmental pollutions and global warming are becoming serious problem, and it is urgent to find clean and renewable energy to substitute the fossil fuels.

Solar energy is a clean, sustainable, wide-distributed energy. The total amount of solar energy is very huge. The amount of sunlight striking the earth's atmosphere continuously is 1.75×10^5 TW, even if 1% of it could be converted into electric energy with a 10% efficiency, it would produce 175 TW, much larger than the total global energy needs predicted to be 25-30 TW in 2050 [1]. But at the same time, solar energy has some disadvantages for its low flux density and large fluctuation due to daily and seasonal variations exacerbated by variations owing to weather. Concentrated solar power (CSP) technology has the ability to overcome these disadvantages and believed to be the future power generation technology.

There are 4 common forms of CSP technologies, parabolic trough, dish Stirlings, concentrating linear Fresnel receiver, and solar power tower. Different types of collectors and different technologies for electricity generation are suitable for different working temperature zones with different costs. Combination of different collectors with different technologies may provide a new direction to achieve higher efficiency with lower cost for CSP.

Cau [2] reported a comparative performance analysis of CSP plants using parabolic trough and linear Fresnel collectors, thermal oil as heat transfer fluid and an Organic Rankine Cycle (ORC) power generation unit. A two-tank direct thermal storage system are included and in the Rankine cycle, regenerator, 4 6 steam extractions and air-cooler condenser are used. The performance analysis of the two types of system shows that CSP plants based on linear Fresnel collectors lead to higher values of electrical energy production per unit area of land and CSP plants based on parabolic troughs gives better values of energy production per unit area of collector.

Franchini [3] carried out simulations to predict the performance of a Solar Rankine Cycle (SRC) and an Integrated Solar Combined Cycle (ISCC) when combined with two different solar field configurations based on parabolic trough collectors (PTCs) and power tower (PT) systems. The comparative analysis was mainly focused on the influence of CSP technology on global solar energy conversion efficiency of both SRC and ISCC plants. Results show that both higher collection efficiency and conversion efficiency of ST compared to PTCs in both SRC and ISCC situations.

Cipollone [4] discussed some thermodynamic and engineering aspects concerning the use of parabolic troughs for heating gasses of gas turbines. They further discussed the Discrete Ericsson Cycle (DEC), in the cycle, a sequence of

intercooled compressions and reheated expansions is deployed to increase cycle specific work and efficiency. They applied optimization adopting as design parameter the power per unit of collector length, and pointed out that the number of compressions and expansions could not exceed three stages.

Behar [5] reviewed the R&D activities and published studies on integrated solar combined cycle system (ISCCS), various configurations have been proposed with their performance investigated. The paper also introduced lots of software or mathematical programs to simulate the performance of various design.

Ghaem [6] investigated and compared the performance of various configurations of hybrid solar dish-Brayton cycle. A thermodynamic model implemented in Engineering Equation Solver (EES) is developed for various configurations. Results show that the model in which receiver located before the turbine can achieve higher performance compare to the one in which the receiver located after the turbine. Simulation of the models pointed out that a comprehensive well defined control algorithm is a vital issue in order to control engine operation, solar input heat flux and sun tracking system.

In this paper, an idea of cascade collection and cascade utilization of solar energy with higher efficiency is presented. Parabolic trough collectors are used to collect lower temperature energy with lower cost and dish collectors are used to collect higher temperature energy with higher efficiency. Rankine cycle is used to work in lower temperature zone and Stirling cycle is used to work in higher temperature zone. Furthermore, effective topological structures are considered to take full advantages of thermodynamic characters of different components of the system. The Stirling engines are cooled by condensed fluid of Rankine cycle to use the heat released by Stirling engines.

First, the idea of cascade system is presented and the feasibility analysis of the system is performed. A conceptual sketch of the system is presented with some important state points. Second, based on this sketch, some components are chosen and some key parameters of the system are given. Third, models of components are built according to their thermodynamic properties. Models of different circuits are built with these component models and efficiency can be obtained by the circuit data. Fourth, two separate systems, dish-Stirling system and trough-Rankine system, are built for comparison. At last, the models of the systems are calculated and results are analysed.

2 System description and specification

In the cascade system, dish collectors are used to provide heat for Stirling engines and air-to-water heat exchanger. Trough collectors are used to provide heat for preheating, evaporating and superheating in the Rankine cycle. Figure 1 shows the sketch of the cascade system. Water is used as the working fluid of Rankine cycle, which is heated in the cold chamber of Stirling engines, pre-heater, evaporator, superheater, and air-to-water heat exchanger successively, and then expand in turbine, condense in condenser. Pumps are used to change the pressure of fluids. Stirling engines are used for power generation and cooled

by feed water of the Rankine cycle. State number pairs of different fluids are marked on the sketch. The first number of a number pair indicates the type of the fluid, the second number of a number pair indicates the state point of the fluid. Number pairs with solid circle indicate saturated liquid states ($x = 0$), and with dotted circle indicates saturated gas states ($x = 1$). Figure 2 shows the T-s diagram of the water circuit in the cascade system. In this Rankine cycle, the heat released in process 2,5-2,6 can be utilized by series of Stirling engines, which may increase the power of Rankine cycle. Figure 3 shows the heat transfer diagram of this process.

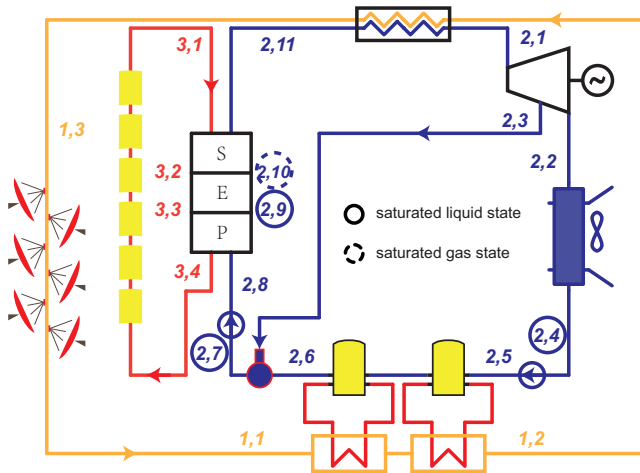


Figure 1: Sketch of the cascade system

To build the cascade system model, several simplifying assumptions are made:

- Steady state at nominal load of the system is analyzed
- Pressure drop due to flow is negligible
- The leak of working fluid in the pipes is neglected
- Same isentropic efficiency of steam turbine with different loads and in different stages
- Heat loss that occurs from the tube to the atmosphere is not considered
- There is no heat loss to the environment for Stirling engines
- Simple models are used of some processes and equipments

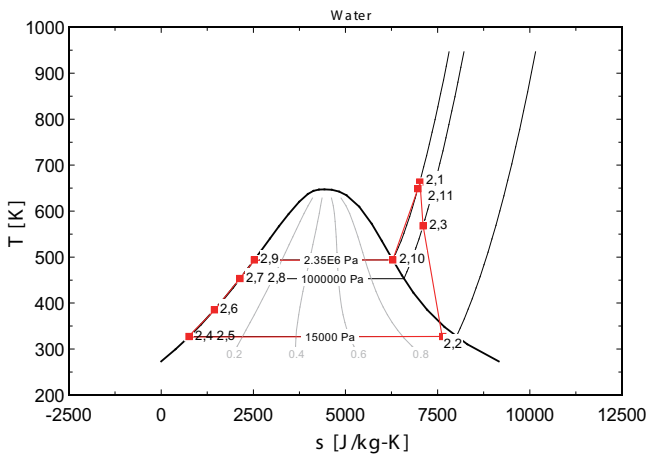


Figure 2: $T - s$ diagram of the water circuit

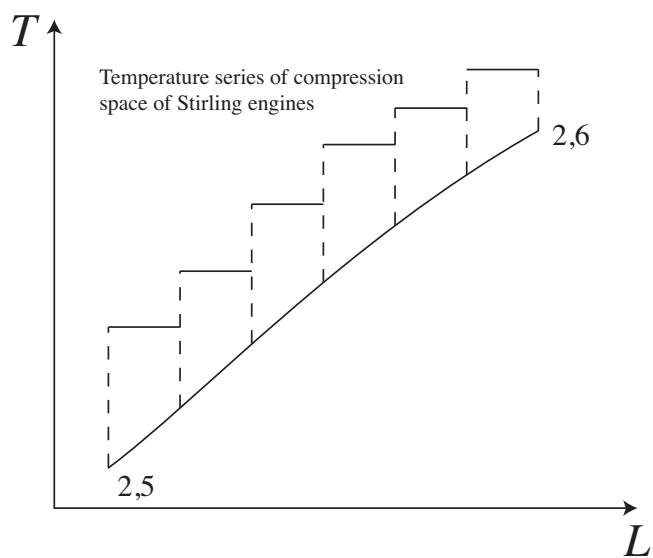


Figure 3: Heat transfer diagram of process 2,5-2,6

- A symmetrical regenerator behaviour is assumed so that a single effectiveness can be defined as $e = \frac{T_R - T_L}{T_H - T_L}$ [7, 8]

Table 1 shows the basic design parameters of the cascade system.

Table 1: Basic design parameters of the cascade system

Parameters	Value
I_r	700 W/m ²
T_{amb}	293 K
p_{amb}	1×10^5 Pa
v_w	4 m/s
P_{ge}	6×10^6 W
$T_{dr,i}$	623 K
$T_{dr,o}$	1073 K
p_{dr}	5×10^5 Pa
$\Delta T_{3,2,min}$	15 K
$T_{tr,o}$	623 K
p_{tr}	2×10^6 Pa
$T_{1,ses,o}$	673 K
n_{se}	100
$T_{tb,s}$	340°C
$p_{tb,s}$	2.35×10^6 Pa
$p_{tb,c}$	1.5×10^4 Pa
$T_{tb,s,d}$	390°C
p_{da}	1×10^6 Pa

3 System model

An EES model was built to investigate the characteristics of the cascade system. The cascade system is built in several blocks. These blocks are made of circuits with efficiency calculations. Three circuits, air circuit, water circuit and oil circuit, are built with some specific state parameters in some key components. Energy-based models of these key components are created on the basis of their thermodynamic behavior, heat transfer and the second law.

The following parts introduce models of some key components.

3.1 Dish collector

The most complicate part of the dish collector is the dish receiver. In our cascade system, the structure of the dish receiver is as shown in Figure 4. This section mainly describes dish receiver.

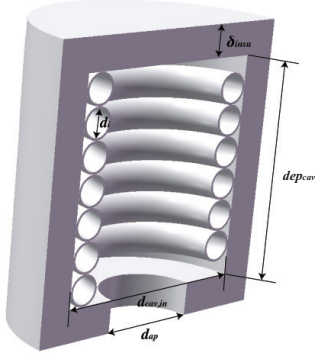


Figure 4: Structure of the dish receiver

Fraser, in his dissertation [9], built a performance prediction model of Stirling dish system with detailed description. The model is also used in the software SAM, which provides performance and financial models for facilitate decision in the renewable energy industry. The dish collector model in the dissertation considers various heat losses, which is a good reference for the dish receiver model of the cascade system.

A dish collector product of SES used in Fraser's dissertation, which is also used in this system, and its parameters are listed in Table 2 [9].

The dish receiver model concerns the losses include: collector losses due to mirror reflectivity, receiver intercept losses, losses due to shading, and thermal losses. Thermal losses take the largest portion of all those losses, which are due to conduction, convection and radiation. Figure 5 shows the heat network of dish receiver, which concerns the losses:

- Radiation losses reflected off of the receiver cavity surfaces and out of the receiver through the aperture. ($q_{rad,ref}$)
- Conductive losses through the receiver insulating layer. ($q_{cond,tot}$)
- Natural convection from the cavity in the absence of wind. ($q_{conv,nat}$)
- Forced convection in the presence of wind. ($q_{conv,for}$)
- Emission losses due to thermal radiation emitted from the receiver aperture. ($q_{rad,emit}$)

Table 2: Parameters of the dish collector

Parameters	Value
d_{cav}	0.46 m
δ_{ins}	0.075 m
dep_{cav}	0.23 m
d_{ap}	0.184 m
k_{ins}	0.06 W/(m·K)
ϵ_{ins}	0.6
α_{cav}	0.87
δ_a	0.005 m
$d_{dr,i}$	0.07 m
A_{dc}	87.7 m ²
θ_{dr}	45°
γ	0.97
$\eta_{shading}$	0.95
ρ	0.91

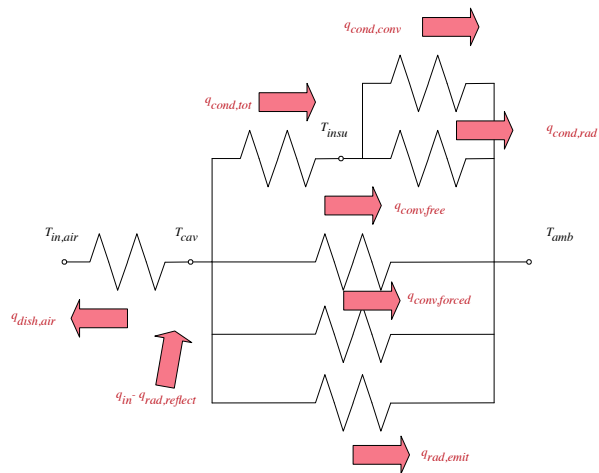


Figure 5: Heat network of dish receiver

$q_{dr,1}$ can be written as

$$q_{dr,1} = h_{dr,1} A_{dr,1} \Delta T_{ln,dr,1}$$

where

$$h_{dr,1} = Nu_{dr,1} k_{dr,1} / d_{dr,i}$$

$$Nu_{dr,1} = c_r Nu'_{dr,1}$$

For helical spiral pipe, multiplier c_r based on curvature ratio can be written as [10]

$$c_r = 1 + 3.5 \frac{d_{dr,i}}{d_{cav} - d_{dr,i} - 2\delta_a}$$

$Nu'_{dr,1}$ is the Nusselt number of straight circular tube, which can be obtained by [11]

$$Nu'_{dr,1} = 0.027 Re_{dr,1}^{0.8} Pr_{dr,1}^{1/3} (\mu_{dr,1}/\mu_{cav})^{0.14}$$

$$c_r = 1 + 3.5 \frac{d_{dr,i}}{d_{cav} - d_{dr,i} - 2\delta_a}$$

and $\Delta T_{ln,dr,1}$ can be written as

$$\Delta T_{ln,dr,1} = \frac{(T_{cav} - T_{dr,i}) - (T_{cav} - T_{dr,o})}{\ln \frac{T_{cav} - T_{dr,i}}{T_{cav} - T_{dr,o}}}$$

To get $q_{dr,1}$, T_{cav} is required. As shown in Figure 5, we need to solve the heat network.

$$q_{in} = q_{rad,ref} + q_{dr,1} + q_{cond,tot} + q_{conv,tot} + q_{rad,emit} \quad (1)$$

q_{in} and η_{dc} can be obtained by

$$q_{in} = I_r \cdot A_{dc} \gamma \eta_{shading} \rho \quad (2)$$

$$\eta_{dc} = q_{dr,1} / (I_r \cdot A_{dc}) \quad (3)$$

Other losses are presented in following sections.

3.1.1 Reflected loss of dish receiver

To determine the reflected loss of the cavity surfaces of the dish receiver $q_{rad,ref}$, the effective absorptance of the cavity receiver α_{eff} is required to determine the fraction of energy reflected out of the receiver. The effective absorptance of a cavity receiver without a receiver aperture cover is given by Equation (4) where α_{cav} is the cavity surface absorptance, A_a is the cavity aperture area, and A_{cav} is the total inner surface area of the cavity [12]. Sandra National Laboratories gave an estimate value of the absorptance of the cavity surface α_{cav} of an existing Stirling dish receiver to be 0.87 [13]. To achieve higher effective absorptance, a smaller ratio of the two surface area should be used. But the ratio is constrained by the concentration ratio of the receiver.

$$\alpha_{eff} = \frac{\alpha_{cav}}{\alpha_{cav} + (1 - \alpha_{cav})(A_{ap}/A_{cav})} \quad (4)$$

$$q_{rad,ref} = q_{in}(1 - \alpha_{eff})$$

3.1.2 Conduction loss of dish receiver

Conduction loss of dish receiver $q_{cond,tot}$ equals to the different two parts: convection loss from the insulating layer to the atmosphere $q_{cond,conv}$ and radiation loss from the insulating layer to the atmosphere $q_{cond,rad}$. Both of the two parts are related to the temperature of insulating layer T_{ins} .

$$\begin{aligned} q_{cond,tot} &= \frac{T_{cav} - T_{ins}}{\ln \frac{d_{cav} + 2\delta_{ins}}{d_{cav}} / (2\pi k_{ins} dep_{cav})} \\ q_{cond,conv} &= h_{ins} A_{ins} (T_{ins} - T_{amb}) \\ &= \frac{k_{ins} Nu_{ins} A_{ins} (T_{ins} - T_{amb})}{d_{cav} + 2\delta_{ins}} \end{aligned}$$

where Nu_{ins} can be obtained by the correlation for flow over a circular cylinder. [14]

$$q_{cond,rad} = \epsilon_{ins} A_{ins} \sigma (T_{ins}^4 - T_{amb}^4)$$

And

$$q_{cond,tot} = q_{cond,conv} + q_{cond,rad}$$

3.1.3 Convection loss of dish receiver

Ma [15] conducted tests to determine the free convection losses from the receiver for alternative setups, and the data were consistent with Stine and McDonald's free convection correlation. It is assumed that forced convection is independent of free convection in the receiver, so the total convection losses can

be represented as the sum of the free and forced convection losses as shown in Figure 5.

$$q_{con,tot} = (h_{nat} + h_{for})A_{cav}(T_{cav} - T_{amb})$$

where $h_{nat} = k_{film}Nu_{nat}/\overline{d_{cav}}$, $\overline{d_{cav}} = d_{cav} - 2d_{tr,i} - 4\delta_a, d_{tr,i} = 0.066 \text{ m}$.

Wu [16] present a comprehensive review and systematic summarization of convection heat loss from cavity receiver in parabolic dish solar thermal power system. And we choose the correlation presented by Leibfried [17]. This correlation gives an extended model of Koenig [18] and Stine [19] with better results.

For forced convection loss, side-on wind convection loss model given by Ma [15], which is independent of the aperture orientation, is used

$$h_{for} = 0.1967v_w^{1.849}$$

3.2 Trough collector

LS-3 is used as the trough collector, its sketch is shown in Figure 6, its parameters are listed in Table 3.

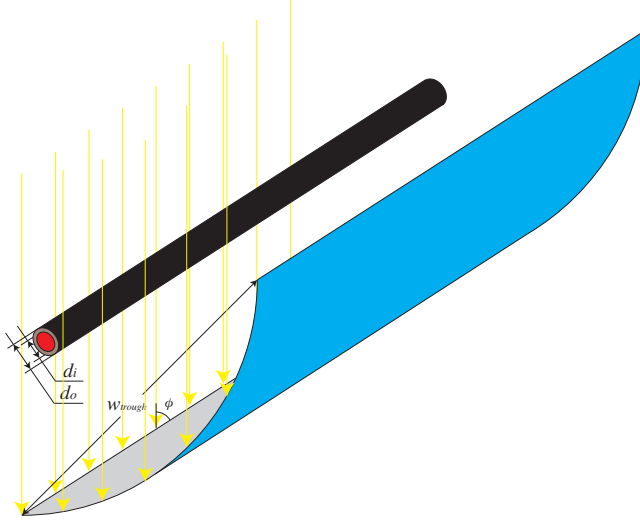


Figure 6: Sketch of trough collector

$$q'' = I_r w_{tc} \eta_{opt,0} K(\phi_{tc}) F_e / P$$

where $P = \pi d_{tr,o}$, $K(\phi)$ is the incidence angle modifier, $\eta_{opt,0}$ is peak optical efficiency (optical efficiency with an incidence angle of 0).

Table 3: Parameters of the trough receiver

Parameters	Value
A_{tc}	545 m ²
w_{tc}	5.76 m
$d_{tr,i}$	0.066 m
$d_{tr,o}$	0.07 m
ρ_{tc}	0.94
γ_{tc}	0.93
τ_{tc}	0.95
α_{tc}	0.96
F_{tc}	0.97
ϕ_{tc}	70°

Assume overall heat transfer coefficient $U(T_{abs})$ is uniform for whole length, so that we can use the heat transfer correlation in Appendix B.

$$\frac{T_{tr,o} - T_{amb} - \frac{q''}{U(T_{abs})}}{T_{tr,i} - T_{amb} - \frac{q''}{U(T_{abs})}} = \exp\left(-\frac{U(T_{abs})PL}{q_{m,3}c_{p,tr}}\right) \quad (5)$$

Since the Nu in the pipe is very large (about 1×10^4), small temperature difference exists between the absorber and oil. So $(T_{tr,i} + T_{tr,o})/2$ can be used as the average value of T_{abs} , and $U(T_{abs})$ can be obtained by the a second-order polynomial function given by Romero[20]. Then using Equation (5), we can get the length L required to get the required number of trough collectors in a row.

The efficiency of the trough collector

$$\eta_{tc} = \frac{q_{m,3}(h_{tr,o} - h_{tr,i})}{I_r w_{tc} L}$$

3.3 Stirling engine array

Stirling engine array is used in the cascade system, Figure 7 shows the layout of the Stirling engine array. Each Stirling engine in the Stirling engine array has the identical parameters: $U_{se,1} = 30 \text{ W/m}^2\cdot\text{K}$, $U_{se,2} = 150 \text{ W/m}^2\cdot\text{K}$, $A_{se,1} = 6 \text{ m}^2$, $A_{se,2} = 6 \text{ m}^2$, $k_{se} = 1.4$, $\gamma_{se} = 3.375$, $n_g = 7.84 \times 10^{-2} \text{ mol}$, $s_{se} = 10 \text{ s}^{-1}$.

Depending on the flow directions of heating and cooling flows, there are two flow types: parallel flow and counter flow. Figure 8 and Figure 9 show the heat transfer diagrams of the two flow types.

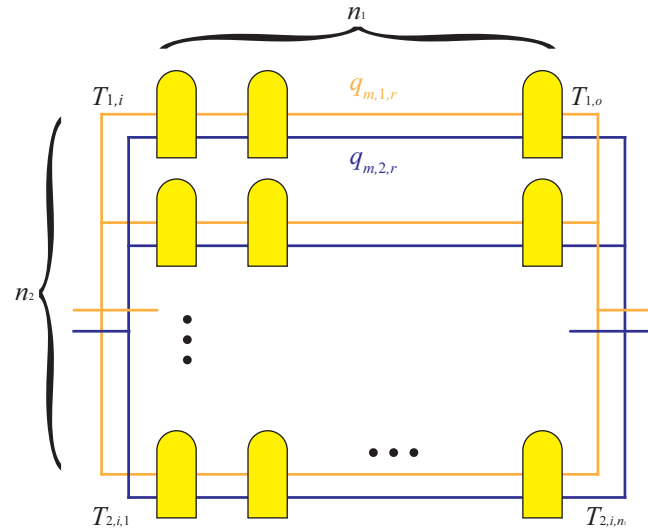


Figure 7: Layout of Stirling engines

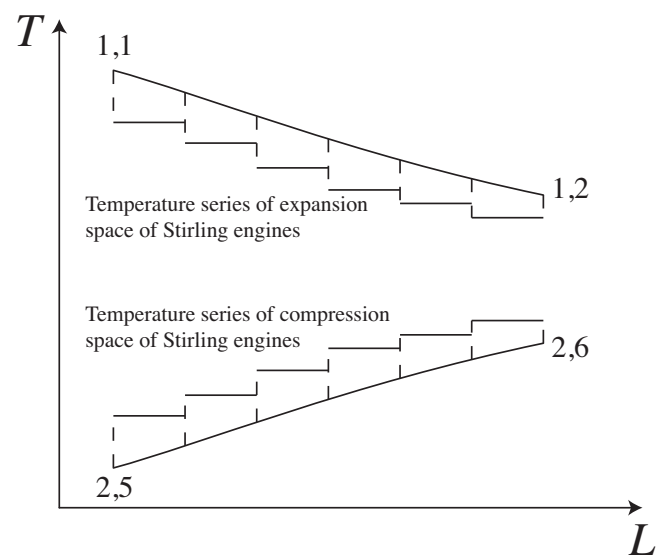


Figure 8: Heat transfer diagram of parallel flow

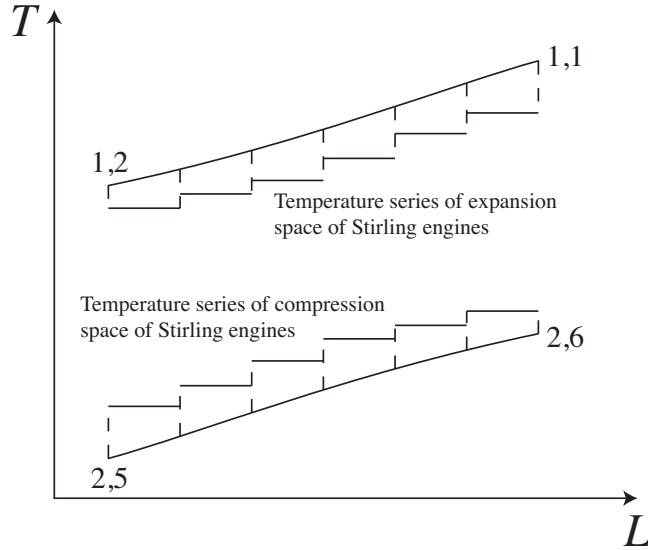


Figure 9: Heat transfer diagram of Counter flow

In Figure 7, $T_{1,i,1} = T_{1,i}$, $q_{m,1,r} = q_{m,1}/n_2$. For x from 1 to $n_1 - 1$, where x is the column number of Stirling engines, $T_{1,i,x+1} = T_{1,o,x}$, $T_{2,i,x+1} = T_{2,o,x}$.

Assume that the positive flow direction is to the right, for parallel flow,

$$T_{2,i,1} = T_{2,i}$$

$$q_{m,2,r} = q_{m,2}/n_2$$

for counter flow,

$$T_{2,o,n_1} = T_{2,i}$$

$$q_{m,2,r} = -q_{m,2}/n_2$$

For a Stirling engine in column x , x from 1 to n_1 , according to Appendix C,

$$T_{H,x} = T_{1,i,x} - \frac{T_{1,i,x} - T_{1,o,x}}{1 - \exp\left(-\frac{U_{se,1}A_{se,1}}{q_{m,1,r}c_{p,1,x}}\right)}$$

$$T_{L,x} = T_{2,i,x} - \frac{T_{2,i,x} - T_{2,o,x}}{1 - \exp\left(-\frac{U_{se,2}A_{se,2}}{q_{m,2,r}c_{p,2,x}}\right)}$$

Assuming a linear temperature profile across the regenerator, the mean effective temperature $T_{R,x} = \frac{T_{H,x} - T_{L,x}}{\ln(T_{H,x}/T_{L,x})}$ [21, 22], and the symmetrical regenerator behaviour assumption $e_x = \frac{T_{R,x} - T_{L,x}}{T_{H,x} - T_{L,x}}$ [7, 8], then the efficiency of each Stirling engine in column x can be written as [23, 1]

$$\eta_{se,x} = \frac{T_{H,x} - T_{L,x}}{T_{H,x} + \frac{1 - e_x}{k - 1} \cdot \frac{T_{H,x} - T_{L,x}}{\ln \gamma_{se}}}$$

For energy balance,

$$q_{m,1,r}(h_{1,i,x} - h_{1,o,x})(1 - \eta_{se,x}) = q_{m,2,r}(h_{2,o,x} - h_{2,i,x})$$

And the power of Stirling engine in column x can be written as

$$n_g R (T_{H,x} - T_{L,x}) s_{se} \ln \gamma_{se} = q_{m,1,r}(h_{1,i,x} - h_{1,o,x}) \eta_{se,x}$$

By solving above equations, efficiency of the Stirling engine array η_{se} can be obtained by

$$\eta_{se} = 1 - \frac{q_{m,2}(h_{2,o,n_1} - h_{2,i,1})}{q_{m,1}(h_{1,i,1} - h_{1,o,n_1})}$$

and power of each Stirling engine in column x

$$P_{se,x} = q_{m,1,r}(h_{1,i,x} - h_{1,o,x}) \eta_{se,x}$$

and power of the Stirling engine array

$$P_{se} = \eta_{se} q_{m,1}(h_{1,i,1} - h_{1,o,n_1})$$

3.4 Steam turbine

A steam turbine product, N-6 2.35, of Qingdao Jieneng Power Station Engineering Co., Ltd is used for calculation. Its isentropic efficiency $\eta_{tb,i}$ can be obtained by the given design parameters.

Using basic design parameters in Table 1, parameters of state 2,2 and 2,3 in Figure 1 of the steam turbine can be obtained by the following equations.

$$\eta_{tb,i} = \frac{h_{2,1} - h_{2,2}}{h_{2,1} - h_{i,2,2}}$$

$$\eta_{tb,i} = \frac{h_{2,1} - h_{2,3}}{h_{2,1} - h_{i,2,3}}$$

The output power of steam turbine

$$P_{tb} = (1 - y) q_{m,2} (h_{2,1} - h_{2,2}) + y q_{m,2} (h_{2,1} - h_{2,3})$$

The sum power of pumps

$$P_{pu} = (1 - y) q_{m,2} (h_{2,5} - h_{2,4}) + q_{m,2} (h_{2,8} - h_{2,7})$$

Heat injected in the water circuit

$$Q_2 = (1 - y) q_{m,2} (h_{2,6} - h_{2,5}) + q_{m,2} (h_{2,1} - h_{2,8})$$

The efficiency of Rankine cycle can be expressed as

$$\eta_{rankine} = (P_{tb} - P_{pu}/\eta_{ge})/Q_2$$

4 Separate system models

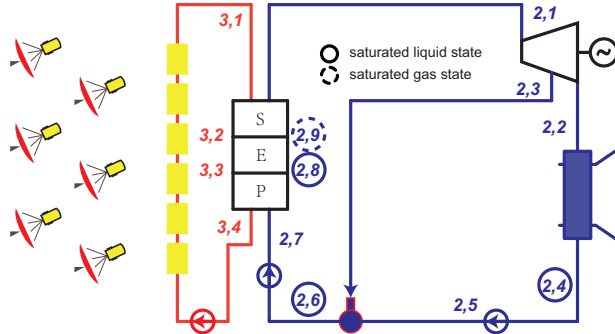


Figure 10: Sketch of the separate systems

Figure 10 shows the sketch of the separate systems. These two separate systems were built for comparison. They use the same dish collectors and trough collectors with the same thermal efficiencies.

4.1 Separate trough system

Steam turbine has the same main parameters and same isentropic efficiency with that of the cascade system. Pressure of deaerator are the same of the cascade system. So parameters of state 2,2 and 2,3 in Figure 10 of the steam turbine can be obtained by the following equations.

$$\eta_{tb,i} = \frac{h_{2,1,s} - h_{2,2,s}}{h_{2,1,s} - h_{i,2,2,s}}$$

$$\eta_{tb,i} = \frac{h_{2,1,s} - h_{2,3,s}}{h_{2,1,s} - h_{i,2,3,s}}$$

The output power of steam turbine

$$P_{tb,s} = (1 - y_s) q_{m,2,s} (h_{2,1,s} - h_{2,2,s}) + y_s q_{m,2,s} (h_{2,1,s} - h_{2,3,s})$$

The output power of generator

$$P_{ge,s} = P_{tb,s} \eta_{ge}$$

The sum power of pumps

$$P_{pu,s} = (1 - y_s) q_{m,2,s} (h_{2,5,s} - h_{2,4,s}) + q_{m,2,s} (h_{2,7,s} - h_{2,6,s})$$

Heat injected in the water circuit

$$Q_{2,s} = q_{m,2,s} (h_{2,1,s} - h_{2,7,s})$$

The generator efficiency is the same of that in the cascade system, and the efficiency of Rankine cycle can be expressed as

$$\eta_{rankine,s} = (P_{tb,s} - P_{pu,s} / \eta_{ge}) / Q_{2,s}$$

4.2 Separate dish system

In the separate dish system, Stirling engines with the same number of dish collectors are directly put on the focuses of the dish collectors. Water is used for cooling the Stirling engines.

$T_{H,s}$ is chosen to be equal to outlet temperature of air in dish receiver. $T_{L,s}$ is chosen to be 310 K, the default expansion temperature in Fraser's dissertation [9] for the calculation of 4-95 NKII engine. k and γ are chosen the same value as that of the Stirling engines in the cascade system.

$$\begin{aligned} T_{R,s} &= \frac{T_{H,s} - T_{L,s}}{\ln \frac{T_{H,s}}{T_{L,s}}} \\ e_s &= \frac{T_{R,s} - T_{L,s}}{T_{H,s} - T_{L,s}} \\ \eta_{se,s} &= \frac{T_{H,s} - T_{L,s}}{T_{H,s} + \frac{1 - e_s}{k - 1} \cdot \frac{T_{H,s} - T_{L,s}}{\ln \gamma}} \end{aligned}$$

The power of Stirling engines

$$P_{se,s} = n_{dc} A_{dc} I_r \eta_{dc} \eta_{se,s}$$

5 Results and Conclusion

The results presented in Table 4 are issued using design parameters with counter flow of two fluids in Stirling engine array as the default flow type. Different results between two flow types of Stirling engine array are listed in Table 5.

Table 4: Some important results using typical parameters

Parameters	Value
η	0.1974
η_s	0.1962
η_{diff}	0.0062
η_{se}	0.3407
$\eta_{se,s}$	0.3786
$\eta_{rankine}$	0.2660
$\eta_{rankine,s}$	0.2678
P_{ge}	6×10^6 W
$P_{ge,s}$	5.826×10^6 W
P_{se}	3.552×10^5 W
$P_{se,s}$	4.909×10^5 W

Table 5: Results of Stirling engine array with two different flow types

x	Parallel flow				Counter flow			
	$T_{1,i}$ K	$T_{2,i}$ K	P_{se} W	η_{se} -	$T_{1,i}$ K	$T_{2,i}$ K	P_{se} W	η_{se} -
1	1073.15	327.17	5000	0.3648	1073.15	348.09	4867	0.3601
2	1022.38	329.80	4630	0.3599	1023.25	345.48	4541	0.3562
3	974.35	332.29	4280	0.3544	975.82	343.00	4230	0.3520
4	928.90	334.65	3949	0.3485	930.75	340.65	3934	0.3474
5	885.91	336.88	3635	0.3419	887.94	338.42	3654	0.3424
6	845.26	339.00	3338	0.3347	847.28	336.29	3387	0.3370
7	806.82	341.00	3057	0.3269	808.69	334.28	3134	0.3312
8	770.49	342.91	2792	0.3184	772.06	332.37	2894	0.3248
9	736.16	344.71	2541	0.3090	737.31	330.55	2666	0.3180
10	703.75	346.43	2304	0.2989	704.37	328.82	2450	0.3106

5.1 Influence of I_r

It is found that I_r can effect the efficiency difference of cascade system and separate systems η_{diff} . Figure 11 shows curve fits of efficiency differences η_{diff} versus I_r with a series of different Stirling engine array power ratios. As it can be seen, for a higher I_r ($I_r > 550 \text{ W/m}^2$), $\eta_{diff} > 0$, the cascade system can achieve a higher efficiency than corresponding separate systems, and increase β achieve a higher η_{diff} . For a lower I_r ($I_r < 550 \text{ W/m}^2$), increase β may achieve a lower η_{diff} , even a negative η_{diff} . At this situation, the cascade system achieves a lower efficiency than corresponding separate systems, and the higher β , the lower η_{diff} . This means I_r is a key factor to determine whether cascade system should be applied in a certain location.

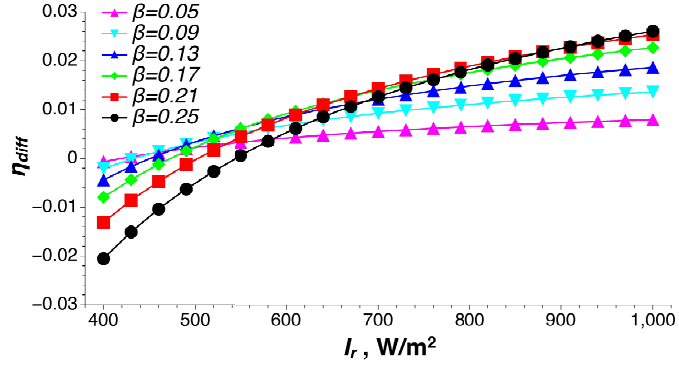


Figure 11: Curve fits of efficiency difference η_{diff} versus I_r

5.2 Influence of β

As it can be seen in Table 4, the η_{diff} is very small with the design parameters given above. A reason η_{diff} to be so small is that β , the ratio of power of Stirling engines to the total power, is very small, the heat released by the Stirling engine array is a small portion of the heat absorbed in the Rankine cycle. So increase β may achieve higher η_{diff} . The relationship between η_{diff} and β under a series of I_r is shown in Figure 12. It can be found that, for a certain β , higher I_r can achieve higher η_{diff} , so a higher I_r location is always more suitable for cascade system. for a higher I_r , increase β may achieve a higher η_{diff} , but there is a limit. For $I_r = 900 \text{ W/m}^2$, the maximum $\eta_{diff} = 0.0228$ appears at $\beta = 0.23$.

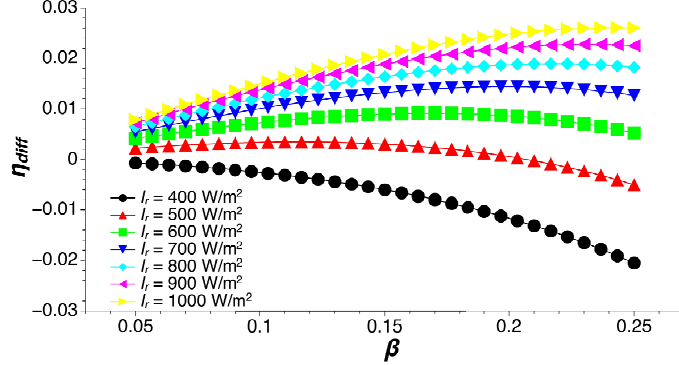


Figure 12: Curve fits of efficiency difference η_{diff} versus β

5.3 Influence of flow type

Flow type between heating and cooling streams can influence the efficiency of Stirling engine array. Parallel flow, compared to counter flow, leads to higher Stirling engine efficiency in the first columns of the array for lower cooling temperature, while lower Stirling engine efficiency in the last columns for higher cooling temperature. Table 5 shows the different results of the two flow types. The fit curves of temperature series of the heating and cooling fluids and the efficiency of Stirling engines in different columns are shown in Figure 13 and 14.

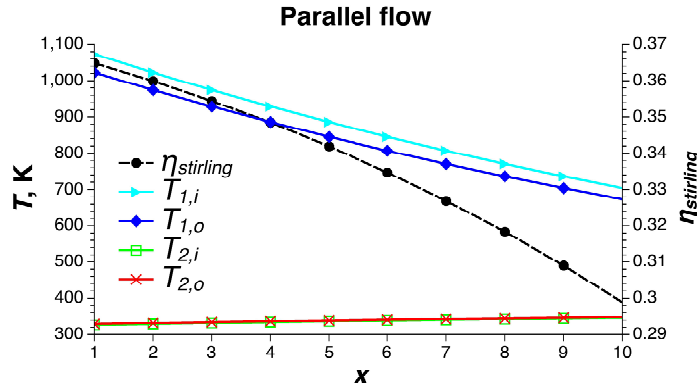


Figure 13: Parallel flow: Temperature series of two fluids and efficiency of Stirling engines in column x

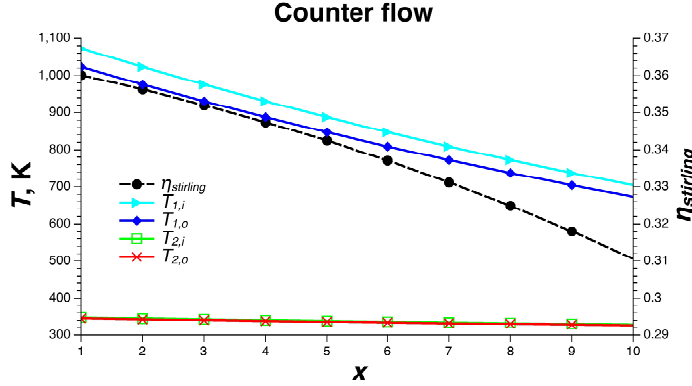


Figure 14: Counter flow: Temperature series of two fluids and efficiency of Stirling engines in column x

From Figure 13 and 14, it can be concluded that the temperature increment of cooling fluid is much smaller than the temperature decrement of heating fluid due to their large difference of $c_p q_m$, which leads to a small difference of overall efficiency of Stirling engine array between the two flow types.

To find out a clear difference of the two flow types, a simple model of Stirling engine array was built with air as the heating fluid and water as the cooling fluid. $T_{1,i}, T_{1,o}, T_{2,i}, q_{1,m}$ are fixed and chosen the same values as in the cascade system. Change the value of $q_{2,m}$, and the corresponding Stirling engine array efficiency of the two flow types can be obtained. Figure 15 shows the efficiency of Stirling engine array with different $q_{2,m}$ in two flow types. It can be found that counter flow has a higher efficiency than parallel flow, and with lower $q_{2,m}$ comes with higher efficiency difference.

For a system with large difference of $c_p q_m$ of two fluids, that means one fluid can only achieve a small ΔT compared to the other fluid, will lead to a small difference of two flow types. For a system with similar difference of $c_p q_m$, use the counter flow can achieve a higher efficiency.

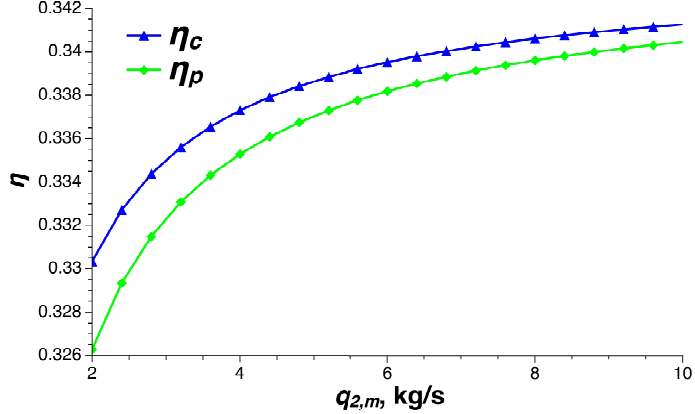


Figure 15: Efficiency of Stirling engine array with different $q_{2,m}$

The first version of cascade system with two different types of collectors and two different power generation methods has been established, including different fluid circuits, with component models. Simulations were carried out and results were compared with corresponding separate systems. Results show that the cascade system can achieve a higher efficiency under certain parameters. The directions to increase the efficiency difference between cascade system and corresponding separate systems were also discussed. higher I_r and β is better for a cascade system. The flow type of fluids for heating and cooling Stirling engine array is also required to concern on designing a relative cascade system. Using a cascade system with a different β can change the portion of dish collector area of total collector area, which can affect the cost of this technique. The cost analysis and optimization research of the cascade system is not included in this paper, which are worthy for further research later.

Nomenclature

\overline{d}_{cav}	Effective diameter of the cavity, m
A	Area, m ²
$A_{se,1}$	Heat transfer area of Stirling engine at air side, m ²
$A_{se,2}$	Heat transfer area of Stirling engine at water side, m ²
c_p	Heat capacity of Stirling engine working gas at constant pressure, J/(kg·K)
c_r	Heat transfer correction factor of coiled tube of volumetric receiver
c_v	Heat capacity of Stirling engine working gas at constant volume, J/(kg·K)
d	Diameter, m
dep	Depth, m
e	Regeneration effectiveness of the Stirling engine
Fe	Soiling factor
I_r	Direct Normal Irradiance, W/m ²
K	Incidence angle modifier of trough collector
k	Thermal conductivity, W/(m·K)
k_{se}	Specific heat ratio of the working gas in Stirling engine
n	Number
n_1	Number of columns of the Stirling engine array
n_2	Number of rows of the Stirling engine array
n_g	Amount of working gas in each Stirling engine, mol
n_{se}	Number of Stirling engines in the Stirling engine array
Nu	Nusselt number
P	Power, W
p	Pressure, Pa
$p_{tb,c}$	Exhaust pressure of turbine, Pa
$p_{tb,s}$	Main steam pressure of turbine, Pa

Pr	Prandtl number
q''	Heat flux, W/m ²
q_{in}	Solar energy launched into dish receiver aperture, W
$q_{m,1,r}$	Mass flow rate of air in each row of Stirling engine array, kg/s
$q_{m,2,r}$	Mass flow rate of water in each row of Stirling engine array, kg/s
q_m	Mass flow rate, kg/s
Re	Reynolds number
s_{se}	Speed of Stirling engine, s ⁻¹
T_H	Highest temperature of expansion space, K
T_L	Lowest temperature of compression space, K
T_R	Regenerator temperature, K
$T_{1,ses,o}$	Air temperature after heating Stirling engine, K
$T_{tb,s,d}$	Designed mean steam temperature of turbine, K
$T_{tb,s}$	Main steam temperature of turbine, K
U	Overall heat transfer coefficient, W/(m ² .K)
$U_{se,1}$	Overall heat transfer coefficient of Stirling engine at air side, W/(m ² .K)
$U_{se,2}$	Overall heat transfer coefficient of Stirling engine at water side, W/(m ² .K)
v_w	Ambient wind speed, m/s
w_{tc}	Width of trough collector, m
x	Dryness fraction
y	Extraction rate of steam turbine

Abbreviations

EES	Engineering Equation Solver
SAM	System Advisor Model
SES	Stirling Energy System

Greek Symbols

α	Absorptance
β	Ratio of power of Stirling engines to the total output power of cascade system
δ	Thickness, m
δ_a	Thickness of air tube in volumetric receiver, m
$\Delta T_{3,2,min}$	Minimum temperature difference between oil and water in the oil-to-water heat exchanger, K
ϵ	Emissivity
η	Efficiency of cascade system
η	Efficiency
η_s	Efficiency of separate systems
$\eta_{opt,0}$	Optical efficiency with an incidence angle of 0
$\eta_{shading}$	Shading factor
γ	Intercept factor
γ_{se}	Compression ratio of Stirling engine
μ	Viscosity, kg/(m·s)
ϕ_{tc}	Incidence angle of trough collector, rad
ρ	Reflectivity
θ_{dr}	Dish collector aperture angle, rad (0 is horizontal, $\pi/2$ is vertically down)

Subscripts

ap	Aperture of the dish receiver
cav	Cavity of the dish receiver
$cond$	Conduction
$conv$	Convection
da	Deaerator
dc	Dish collector
$diff$	Difference between cascade system and separate systems
dr	Dish receiver

<i>eff</i>	Effective parameter of the dish receiver cavity
<i>emit</i>	Emitted radiation
<i>for</i>	Forced convection
<i>i</i>	Inlet
<i>i</i>	Inner
<i>i</i>	Isentropic
<i>ins</i>	Insulating layer of the dish receiver
<i>nat</i>	Nature convection
<i>o</i>	Outer
<i>o</i>	Outlet
<i>rad</i>	Radiation
<i>ref</i>	Reflected radiation
<i>s</i>	Separate systems
<i>se</i>	Stirling engine
<i>ses</i>	Stirling engine array
<i>tb</i>	Steam turbine
<i>tc</i>	Trough collector
<i>tr</i>	Trough receiver
<i>x</i>	Stirling engine in column <i>x</i>
1	First fluid, Air
2	Second fluid, Water

References

- [1] D.Y. Goswami. *Principles of Solar Engineering, Third Edition*. CRC Press, 2015.
- [2] Giorgio Cau and Daniele Cocco. Comparison of medium-size concentrating solar power plants based on parabolic trough and linear Fresnel collectors. *Energy Procedia*, 45(0):101–110, 2014.
- [3] G. Franchini, A. Perdichizzi, S. Ravelli, and G. Barigozzi. A comparative study between parabolic trough and solar tower technologies in Solar Rankine Cycle and Integrated Solar Combined Cycle plants. *Solar Energy*, 98(PC):302–314, 2013.
- [4] Roberto Cipollone, Andrea Cinocca, and Angelo Gualtieri. A new conversion section for parabolic trough - Concentrated Solar Power (CSP-PT) plants. In *Energy Procedia*, volume 45, pages 61–70, 2014.
- [5] Omar Behar, Abdallah Khellaf, Kamal Mohammedi, and Sabrina Ait-Kaci. A review of integrated solar combined cycle system (ISCCS) with a parabolic trough technology. *Renewable and Sustainable Energy Reviews*, 39(0):223–250, 2014.
- [6] Sara Ghaem. Modeling and Analysis of Hybrid Solar-Dish Brayton Engine. *SolarPACES Conference*, 2012.
- [7] F. Formosa and G. Despesse. Analytical model for Stirling cycle machine design. *Energy Conversion and Management*, 51(10):1855–1863, 2010.
- [8] A.J. Juhasz. A mass computation model for lightweight brayton cycle regenerator heat exchangers. In *8th Annual International Energy Conversion Engineering Conference*, 2010.
- [9] P.R. Fraser. *Stirling dish system performance prediction model*. Madison, 2008.
- [10] Pablo Coronel and K. P. Sandeep. Heat transfer coefficient in helical heat exchangers under turbulent flow conditions. *International Journal of Food Engineering*, 4(1), 2008.
- [11] R W Serth. *Process heat transfer principles and applications*. Elsevier Academic Press, Amsterdam; London, 2007.
- [12] John A. Duffie and William A. Beckman. *Solar Engineering of Thermal Processes: Fourth Edition*. Wiley, 2013.
- [13] R. E. Hogan. AEETES - a solar reflux receiver thermal performance numerical model. *Solar energy*, 52(2):167–178, 1994.

- [14] S. W. Churchill and M. Bernstein. A correlating equation for forced convection from gases and liquids to a circular cylinder in crossflow. *Journal of Heat Transfer*, 99(2):300–306, 05 1977.
- [15] Robert Y Ma. Wind effects on convective heat loss from a cavity receiver for a parabolic concentrating solar collector. *Sandia National Laboratory*, SAND92-7293(September), 1993.
- [16] Shuang-Ying Wu, Lan Xiao, Yiding Cao, and You-Rong Li. Convection heat loss from cavity receiver in parabolic dish solar thermal power system: A review. *Solar Energy*, 84(8):1342 – 1355, 2010.
- [17] U. Leibfried and J. Ortjohann. Convective heat loss from upward and downward-facing cavity solar receivers: Measurements and calculations. *Journal of Solar Energy Engineering*, 117(2):75–84, 05 1995.
- [18] A.A. Koenig and M. Marvin. Convection heat loss sensitivity in open cavity solar receivers. Technical report, Department of Energy, USA, 1981.
- [19] William B Stine and Richard B Diver. A compendium of solar dish/stirling technology. Technical report, DTIC Document, 1994.
- [20] M Romero-Alvarez and E Zarza. Concentrating solar thermal power. *Efficiency and Renewable Energy*, 2007.
- [21] A. Der Minassians. *Stirling Engines for Low-temperature Solar-thermal-electric Power Generation*. University of California, Berkeley, 2007.
- [22] M. Cavazzuti. *Optimization Methods: From Theory to Design Scientific and Technological Aspects in Mechanics*. Springer Berlin Heidelberg, 2012.
- [23] W.B. Stine and R.W. Harrigan. *Solar energy fundamentals and design: with computer applications*. A Wiley-Interscience publication. John Wiley & Sons, Incorporated, 1985.

A Heat transfer to a constant temperature heat source

Constant U, T_c, q_m, c_p , for a given $T_{tr,i}$,

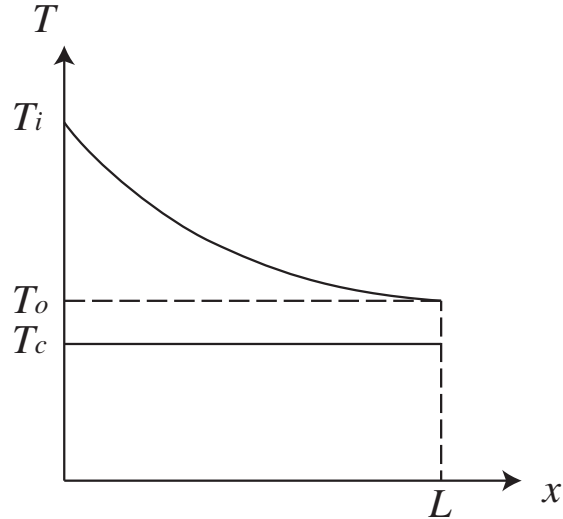


Figure 16: Diagram of heat transfer to a constant temperature heat source

if $A(x) = Px$, x from 0 to L , $T(x)$ from $T_{tr,i}$ to $T_{tr,o}$,

$$q_m c_p dT(x) = (T_c - T(x)) U P dx$$

so,

$$\frac{dT(x)}{dx} = -\frac{UP}{q_m c_p} (T(x) - T_c)$$

Set $F(x) = T(x) - T_c$, then $F(0) = T_{tr,i} - T_c$, and

$$\frac{dF(x)}{F(x)} = -\frac{UP}{q_m c_p} dx$$

$$F(x) = F(0) \cdot \exp\left(-\frac{UP}{q_m c_p} x\right)$$

$$\frac{F(L)}{F(0)} = \exp\left(-\frac{UPL}{q_m c_p}\right)$$

That is

$$\frac{T_{tr,o}-T_c}{T_{tr,i}-T_c}=\exp(-\frac{UA}{q_mc_p})$$

B Ambient loss of a flow under constant heat flux

Constant $U, T_{amb}, q_m, c_p, q''$, for given $T_{tr,i}$,

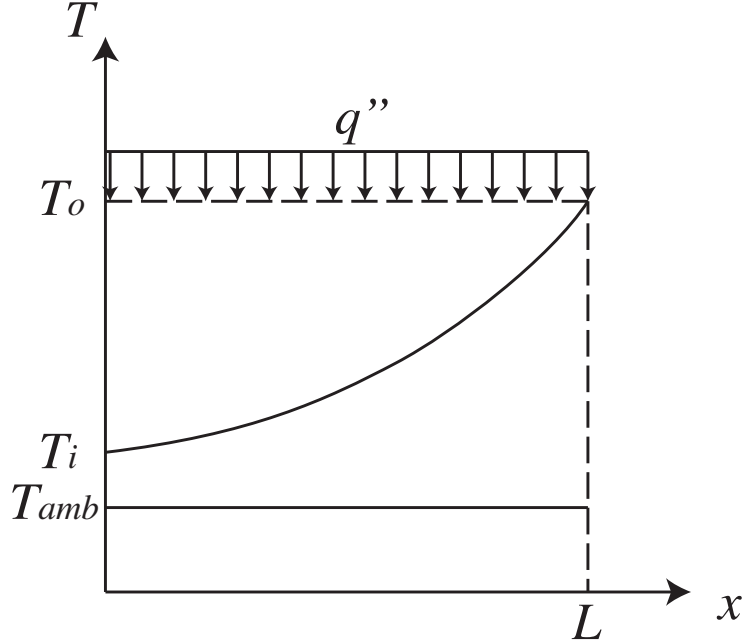


Figure 17: Diagram of ambient loss of a flow under constant heat flux

if $A(x) = Px$, x from 0 to L , $T(x)$ from $T_{tr,i}$ to $T_{tr,o}$,

$$q_m c_p dT(x) = (T_{amb} - T(x)) U P dx + q'' P dx$$

so

$$\frac{dT(x)}{dx} = -\frac{UP}{q_m c_p} T(x) + \frac{q'' P + UPT_{amb}}{q_m c_p}$$

Set $G(x) = T(x) - T_{amb} - \frac{q''}{U}$, then $G(0) = T_{tr,i} - T_{amb} - \frac{q''}{U}$ and

$$\frac{dG(x)}{G(x)} = -\frac{UP}{q_m c_p} dx$$

$$G(x) = G(0) \cdot \exp\left(-\frac{UP}{q_m c_p} x\right)$$

$$\frac{G(L)}{G(0)} = \exp\left(-\frac{UPL}{q_m c_p}\right)$$

That is

$$\frac{T_{tr,o} - T_{amb} - \frac{q''}{U}}{T_{tr,i} - T_{amb} - \frac{q''}{U}} = \exp\left(-\frac{UA}{q_m c_p}\right)$$

C Stirling engine model

A simple Stirling engine model is used for the system. The cycle efficiency is given by [23]

$$\eta = \frac{T_H - T_L}{T_H + \frac{1-e}{k-1} \cdot \frac{T_H - T_L}{\ln \gamma}} \quad (6)$$

where $e = \frac{T_R - T_L}{T_H - T_L}$, T_R is the regenerator temperature, $k = \frac{c_p}{c_v}$ for the working gas, $\gamma_{se} = \frac{V_{max}}{V_{min}}$ is the compression ratio.

The heat transfer diagram is shown in Figure 18. Flow 1 is used for heating the hot chamber of Stirling engine, T_{1i} is the inlet temperature, T_{1o} is the outlet temperature. Flow 2 is used for cooling the cold chamber of Stirling engine, T_{2i} is the inlet temperature, T_{2o} is the outlet temperature. T_H is the highest temperature of expansion space, T_L is the lowest temperature of compression space.

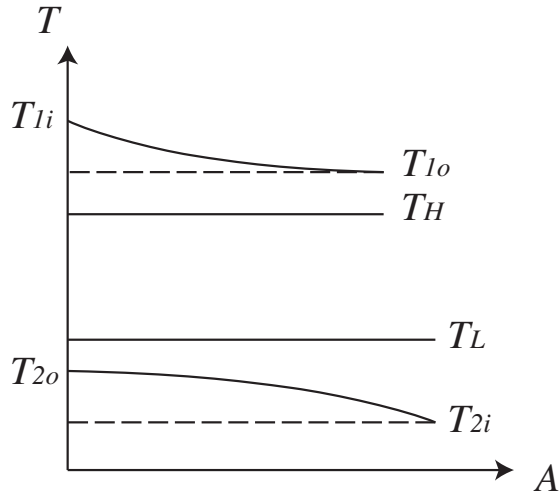


Figure 18: Heat transfer diagram of Stirling engine

According to Appendix A, we have

$$\frac{T_{1o} - T_H}{T_{1i} - T_H} = \exp\left(-\frac{U_1 A_1}{q_{m,1} c_{p1}}\right)$$

and

$$\frac{T_{2o} - T_L}{T_{2i} - T_L} = \exp\left(-\frac{U_2 A_2}{q_{m,2} c_{p2}}\right)$$

So known $T_{1o}, T_{1i}, U_1, A_1, q_{m,1}, c_{p1}, T_{2o}, T_{2i}, U_2, A_2, q_{m,2}, c_{p2}$, we can get T_H and T_L , and then use Equation (6) to get η .